

MULTIPACTOR SIMULATIONS IN 325 MHz SUPERCONDUCTING SPOKE CAVITY FOR AN ELECTRON ACCELERATOR*

T. Kubo[†], T. Saeki, KEK, High Energy Accelerator Research Organization, Tsukuba, Ibaraki, Japan
 E. Cenni, Y. Iwashita, H. Tongu, Kyoto University, Uji, Kyoto, Japan
 R. Hajima, M. Sawamura, Japan Atomic Energy Agency, JAEA, Tokai, Ibaraki, Japan

Abstract

To realize a compact industrial-use X-ray source with the laser-Compton scattering, a 325MHz superconducting spoke cavity for an electron accelerator operated at 4K is under development. Design-optimizations of the first prototype cavity were finished. Multipactor simulations were carried out as parts of optimization efforts. In this paper, procedures of multipactor simulations by using CST studio suite are briefly introduced. Then results of simulations and analyses to extract an optimum geometry are presented. A relation between a cavity geometry and an intensity of multipactor is also commented.

INTRODUCTION

In order to realize an industrial-use laser-Compton scattering compact X-ray source [1, 2], a superconducting cavity for electron acceleration is currently under development [3, 4]. We adopted a 325 MHz superconducting spoke cavity. The spoke cavity [5] has a small diameter around half the wavelength, namely, half a diameter of the elliptic cavity, and make it possible to reduce RF frequency, f_{RF} , with keeping its compactness. By setting $f_{RF} = 325$ MHz, Bardeen-Cooper-Schrieffer (BCS) resistance ($\propto f_{RF}^2$) is significantly reduced, and a cavity dissipation at 4 K nearly equals to that of 1.3 GHz elliptic cavity at 2 K.

The genetic algorithm (GA) known as a method of multi-objective optimization was used to design a spoke cavity by Sawamura et al [3, 4]. Cavities with minimized E_{pk}/E_{acc} and B_{pk}/E_{acc} were generated, from which geometries that maximize the achievable E_{acc} were extracted, where E_{acc} , E_{pk} and B_{pk} are the accelerating field, the peak electric-field and the peak magnetic-field, respectively. There are still degrees of freedom in the detailed design: corner radii of the end-plate and the spoke-base, and so on. Fig. 1 shows examples of geometries optimized by GA, which have similar RF characteristics, but each has different corner radius of the end-plate.

In order to finalize the detailed design, we carried out MP simulations of cavities optimized by GA and extract a model that may suppress a risk of MP as small as possible [6, 7]. In this paper, procedures and results of MP simulations are briefly summarized. Relations between cavity geometries and averaged secondary electron emission yield are also commented.

* The work is supported by Photon and Quantum Basic Research Coordinated Development Program from the Ministry of Education, Culture, Sports, Science and Technology, Japan.

[†] kubitaka@post.kek.jp

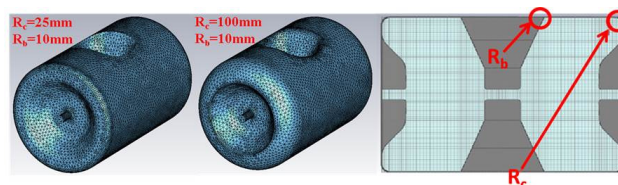


Figure 1: Examples of optimized cavity geometries. Both have optimized geometry and similar RF characteristics, but a detailed design (i.e., a corner radius of the end-plate in this example) is different from each other.

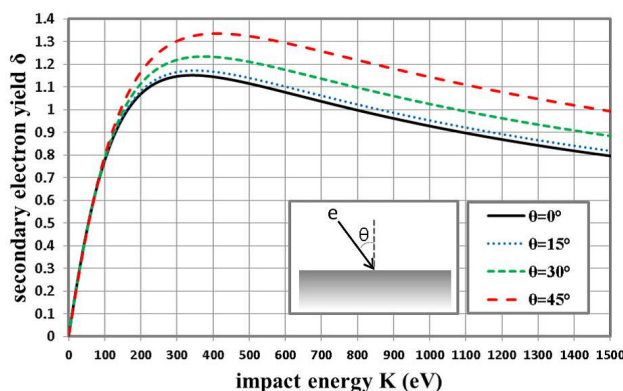


Figure 2: Furman model SEY as functions of impact energy. Each curve corresponds to an impact angle.

SIMULATION PROCEDURE

MP simulations were carried out by using CST studio suite. The procedure is as follows [7, 8, 9].

1. Calculate the electromagnetic-field distribution by using CST MW studio (MWS) Eigenmode solver.
2. Set secondary emission yield (SEY) of a cavity material on CST Particle Studio (PS) (see Fig. 2).
3. Put primary electron sources on a cavity surface. Set a number of primary electrons and their energies $O(10^3)$ and several eV, respectively.
4. Import the electromagnetic-field distribution obtained by MWS, and simulate electron-dynamics by using PS TRK solver (see Fig. 3).

The above procedure is repeated with sweeping E_{acc} and changing models.

In the step 2, we adopted the Furman model [10], in which an SEY is given as a function of the impact energy

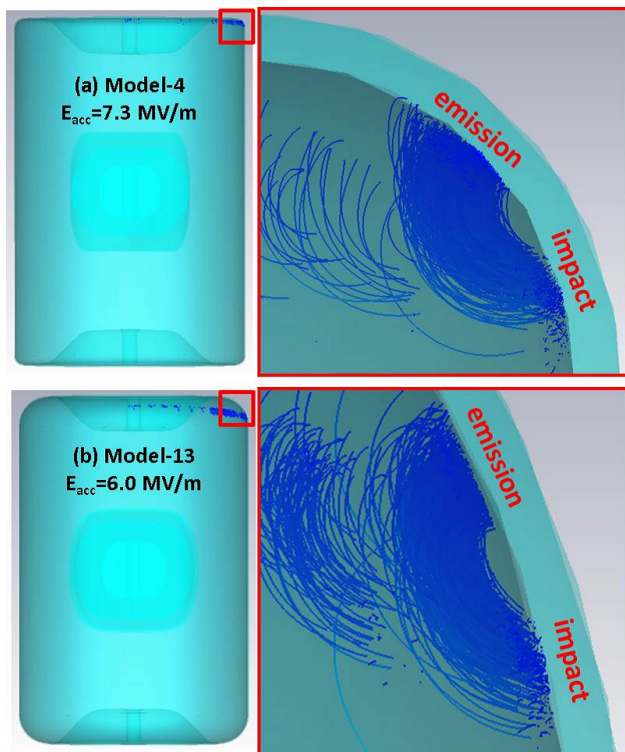


Figure 3: Examples of MP electron trajectories on end-plate corners.

and the impact angle. We are interested in MPs that can not be processed, so-called hard barrier. Thus, at least, an SEY of cavity material must be small enough to suppress MPs in TESLA shape cavity, because we know they are easily processed in a performance test. Material Library equips three types of Nb; Wet Treatment, 300°C Bakeout, and Ar Discharge Cleaned. The material with the smallest SEY among the choices is Ar Discharge Cleaned Nb. Even the SEY of this material leads MPs in TESLA shape cavity and is too large to represent that of real cavity surface. Thus we further reduced the peak value of SEY of Ar Discharge Cleaned Nb to a level that MPs in TESLA shape cavity disappear. Fig. 2 shows the SEY used in the present simulations.

In the step 3, primary electrons are put on the place that MP occurs, i.e., end-plate corner, spoke-base and so on. Even if primary electrons are placed on parts at which no MP occurs, some secondary electrons moves to the place that MP occurs, if it exist, and finally trigger MP, but such a configuration of primary electrons might miss an existence of MP. Putting all primary electrons near the place of MP is recommended.

For an MP analysis, the averaged SEY, $\langle\delta\rangle$, is useful, which gives a direct signal of MP. When MP occurs, $\langle\delta\rangle$ is larger than one. As MP gets heavier, $\langle\delta\rangle$ becomes larger. In CST PS, $\langle\delta\rangle$ can be calculated by $\langle\delta\rangle = \text{SEE current}/\text{Current}$, where the values named Current and SEE current are given in a table named Collision Information [8]. The averaged impact energy, $\langle K\rangle$, is useful to extract information of impacts. When MP occurs, $K_1(\theta) \lesssim$

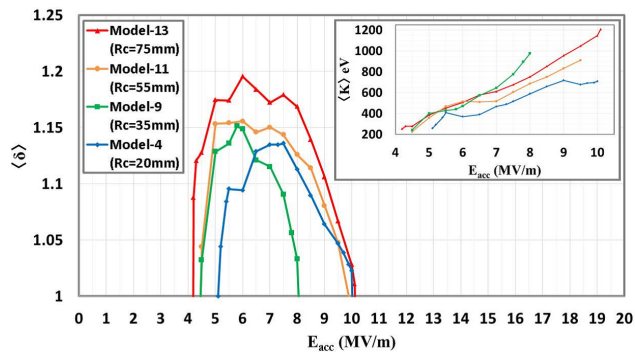


Figure 4: Averaged SEY and averaged impact energy (inset) as functions of E_{acc} for the case that MP occurs near the end-plate corner.

$\langle K\rangle \lesssim K_2(\theta)$ is satisfied, where K_1 and K_2 are the crossover energies ($\delta(K_1) = \delta(K_2) = 1$) and θ is an impact angle. Note that K_1 and K_2 depend on an impact angle (see Fig. 2). In CST PS, $\langle K\rangle$ can be calculated as $\langle K\rangle = \text{Power}/\text{Current}$, where the value named Power is also given in Collision Information [8].

SIMULATION RESULTS

MP at the End-plate Corner

First we carried out MP simulations for models with various corner-radii of end-plates. Model-4, 5, 9, 10, 11, 13, and 6 correspond to $R_c = 20, 25, 35, 45, 55, 75$, and 100 mm, respectively. $R_b = 10$ mm is common among these models. Primary electrons were put on the corner of end-plate, the place that MP occurs.

Fig. 3 shows examples of MP electron trajectories for (a) Model-4 and (b) Model-13. Two-point MPs are seen in both figures. We can see that an impact angle θ is different from each other.

Fig. 4 shows several examples of $\langle\delta\rangle$ as functions of E_{acc} . The inset shows $\langle K\rangle$ as functions of E_{acc} . We can see that E_{acc} inducing MP and the maximum value of $\langle\delta\rangle$ depend on R_c , e.g., MPs occur at $5 \text{ MV/m} < E_{acc} < 10 \text{ MV/m}$ in Model-4 and $4 \text{ MV/m} < E_{acc} < 10 \text{ MV/m}$ in Model-13; the maximum value of $\langle\delta\rangle$ is 1.14 for Model-4 and 1.20 for Model-13. Furthermore a range of $\langle K\rangle$ also depends on R_c , e.g., $2 \times 10^2 \text{ eV} < \langle K\rangle < 7 \times 10^2 \text{ eV}$ in Model-4 and $2 \times 10^2 \text{ eV} < \langle K\rangle < 1.2 \times 10^3 \text{ eV}$ in Model-13.

Fig. 5 shows a width of range of E_{acc} inducing MP (red solid-line) and the maximum value of $\langle\delta\rangle$ (blue dotted-line) as functions of R_c . The width reaches its smallest value when $R_c \approx 35$ mm. $\langle\delta\rangle_{\text{max}}$ increases as R_c increases. We chose Model-9 ($R_c = 35$ mm) as the design of the first prototype.

MP at the Spoke-base

Then we carried out MP simulations of Model-9 ($R_c = 35$ mm) with changing the corner radius of the spoke-base in a range $R_b = 7-15$ mm. Primary electrons were placed on the spoke-base. MP occurs at the spoke-base and tank.

Content from this work may be used under the terms of the CC BY 3.0 licence (© 2015). Any distribution of this work must maintain attribution to the author(s), title of the work, publisher, and DOI.

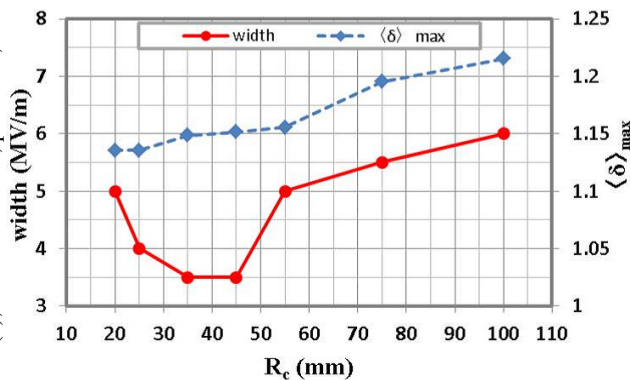


Figure 5: Width of range of E_{acc} inducing MP and the maximum value of $\langle \delta \rangle$ as functions of the corner radius of the end-plate, R_c , for the case that MP occurs near the end-plate corner.

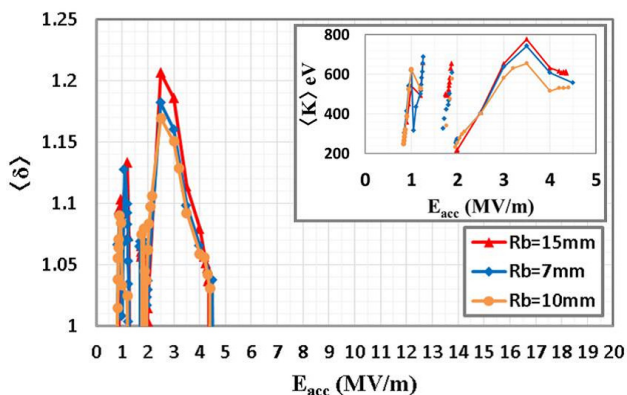


Figure 6: Averaged SEY and averaged impact energy (inset) as functions of E_{acc} for the case that primary electrons are placed near the spoke-base.

Fig. 6 shows $\langle \delta \rangle$ and $\langle K \rangle$ as functions of E_{acc} . Three geometries yielded the similar results. We chose $R_b = 10$ mm as the design of the first prototype.

Some Comments on the Simulation Results

Differences of $\langle \delta \rangle_{\max}$ among the models with different R_c are due to those of the impact angles. For example, $\langle \delta \rangle_{\max}$ of Model-4 ($R_c = 20$ mm) is given by $\langle \delta \rangle_{\max} = 1.14$, which corresponds to the maximum value of δ for $\theta \approx 0^\circ$ (see Fig. 2). On the other hand, $\langle \delta \rangle_{\max}$ of Model-13 ($R_c = 75$ mm) is given by $\langle \delta \rangle_{\max} = 1.20$, which corresponds to the maximum value of δ for $\theta \approx 25^\circ$ (see Fig. 2). A difference of impact angle between Model-4 and Model-13 is explicitly shown in Fig. 3. According to Fig. 2, the crossover energies, K_1 and K_2 , have θ dependences, which are consistent with the result that the range of $\langle K \rangle$ for Model-13 is wider than that for Model-4.

We chose parameters that suppress a risk of MP as small as possible, but, combining Fig. 4 and 6, we find $\langle \delta \rangle > 1$ at almost all E_{acc} below 10 MV/m. Our 7 MV/m operation at 325 MHz [2] may have a difficulty due to the MP. We further investigate the anticipation and continue MP simulations.

SUMMARY

- We are developing a superconducting spoke cavity for the electron acceleration to realize a compact industrial-use X-ray source with the laser-Compton scattering. Geometries of spoke cavities have been optimized by using the genetic algorithm (Fig. 1). To finalize the detailed design, we carried out multipactor simulations.
- Procedures of the multipactor simulation by using CST studio suite and some notes were briefly summarized. In particular, we emphasized that appropriate secondary electron yield should be used for studying the hard barrier. We used SEY of processed Nb that does not induce the multipactor in TESLA shape cavity (Fig. 2).
- We carried out multipactor simulations with changing corner radius of the end-plate (Fig. 4) and found the optimum size of corner radius (Fig. 5). Then the similar simulations were carried out with fixing corner radius of the end-plate and varying that of the spoke-base (Fig. 6). Based on the results, we fixed the design of first prototype cavity.
- We commented on a relation between a multipactor and a corner radius of end-plate. The impact angle (Fig. 3), which depends on a corner radius, significantly affects the intensity of multipactor.

REFERENCES

- [1] R. Hajima, T. Hayakawa, N. Kikuzawa, and E. Minehara, J. Nucl. Sci. Tech. **45**, 441 (2008).
- [2] R. Hajima, M. Sawamura, T. Kubo, T. Saeki, E. Cenni, Y. Iwashita, and H. Tongu, "Development of superconducting spoke cavities for laser Compton scattered X-ray sources", in this proceedings, WEPMA056.
- [3] M. Sawamura, R. Hajima, R. Nagai, T. Kubo, H. Fujisawa, and Y. Iwashita, in *Proceedings of IPAC2014, Dresden, Germany* (2014), p. 1946, WEP0005.
- [4] M. Sawamura, R. Hajima, R. Nagai, and N. Nishimori, in *Proceedings of SRF2011, Chicago, IL USA* (2011), p. 165, MOPO036.
- [5] C. S. Hopper and J. R. Delayen, Phys. Rev. ST Accel. Beams **16**, 102001 (2013).
- [6] Y. Iwashita, H. Fujisawa, H. Tongu, R. Hajima, R. Nagai, M. Sawamura, and T. Kubo, in *Proceedings of IPAC2014, Dresden, Germany* (2014), p. 2543, WEPRI030.
- [7] T. Kubo, E. Cenni, H. Fujisawa, R. Hajima, Y. Iwashita, T. Saeki, M. Sawamura, and H. Tongu, in *Proceedings of LINAC14, Geneva, Switzerland* (2013), p. 1030, THPP075.
- [8] G. Romanov, private communications.
- [9] G. Romanov, in *Proceedings of LINAC08, Victoria, BC, Canada* (2008), p. 166, MOP043.
- [10] M. A. Furman and M. T. F. Pivi, Phys. Rev. ST Accel. Beams **5**, 124404 (2002).